CellPress

Cell Metabolism
Article

Cytoplasmic Tyrosine Phosphatase Shp2 Coordinates Hepatic Regulation of Bile Acid and FGF15/19 Signaling to Repress Bile Acid Synthesis

Shuangwei Li,[1] Diane D.F. Hsu,[1] Bing Li,[2] Xiaolin Luo,[1] Nazilla Alderson,[1] Liping Qiao,[3] Lina Ma,[4] Helen H. Zhu,[1] Zhao He,[1] Kelly Suino-Powell,[5] Kaihong Ji,[1] Jiefu Li,[1] Jianhua Shao,[3] H. Eric Xu,[5,6] Tiangang Li,[7] and Gen-Sheng Feng[1,*]
[1]Department of Pathology, Division of Biological Sciences, University of California, San Diego, La Jolla, CA 92093-0864, USA
[2]Department of Molecular, Cell and Developmental Biology, University of California, Los Angeles, Los Angeles, CA 90095, USA
[3]Department of Pediatrics, University of California, San Diego, La Jolla, CA 92093-0983, USA
[4]Molecular Neuroscience Laboratory, The Salk Institute for Biological Sciences, La Jolla, CA 92186, USA
[5]Laboratory of Structural Sciences, Van Andel Research Institute, 333 Bostwick Avenue Northeast, Grand Rapids, MI 49503, USA
[6]VARI-SIMM Center, Center for Structure and Function of Drug Targets, CAS-Key Laboratory of Receptor Research, Shanghai Institute of Materia Medica, Chinese Academy of Sciences, Shanghai 201203, China
[7]Department of Pharmacology, Toxicology, and Therapeutics, University of Kansas Medical Center, Kansas City, KS 66160, USA
*Correspondence: gfeng@ucsd.edu
http://dx.doi.org/10.1016/j.cmet.2014.05.020

SUMMARY

Bile acid (BA) biosynthesis is tightly controlled by intrahepatic negative feedback signaling elicited by BA binding to farnesoid X receptor (FXR) and also by enterohepatic communication involving ileal BA reabsorption and FGF15/19 secretion. However, how these pathways are coordinated is poorly understood. We show here that nonreceptor tyrosine phosphatase Shp2 is a critical player that couples and regulates the intrahepatic and enterohepatic signals for repression of BA synthesis. Ablating Shp2 in hepatocytes suppressed signal relay from FGFR4, receptor for FGF15/19, and attenuated BA activation of FXR signaling, resulting in elevation of systemic BA levels and chronic hepatobiliary disorders in mice. Acting immediately downstream of FGFR4, Shp2 associates with FRS2α and promotes the receptor activation and signal relay to several pathways. These results elucidate a molecular mechanism for the control of BA homeostasis by Shp2 through the orchestration of multiple signals in hepatocytes.

INTRODUCTION

The biosynthesis of bile acids (BAs) in hepatocytes is a primary pathway for cholesterol catabolism and removal of excess cholesterol via fecal disposal (Chiang, 2002; de Aguiar Vallim et al., 2013; Russell, 2003; Thomas et al., 2008). When secreted into duodenum postprandially, BAs act as "physiological detergent" to emulsify food lipids and facilitate their absorption by intestine. Recently, BAs are also viewed as signaling molecules in several metabolic processes (Houten et al., 2006; Vallim and Edwards, 2009).

Because of its toxicity in excess amounts, BA synthesis is tightly controlled by a negative feedback mechanism. BAs bind farnesoid X receptor (FXR) in hepatocytes (Makishima et al., 1999; Parks et al., 1999) and transactivate small heterodimer partner (SHP) to repress the expression of *Cyp7a1* that encodes cholesterol 7a-hydroxylase, the rate-limiting enzyme for BA synthesis (Lu et al., 2000). *FXR* knockout (KO) mice displayed increased BA levels, higher plasma cholesterol, phospholipids, and triglycerides and were more susceptible to cholesterol-induced hepatic steatosis (Anakk et al., 2011; Sinal et al., 2000). However, *SHP* deletion rendered only a mild increase of the BA pool size in mice (Kerr et al., 2002), and *SHP* KO mice were protected from liver damage induced by cholesterol and BA diet (Wang et al., 2003). These observations suggest SHP-independent pathways in the control of *Cyp7a1* expression. Consistently, *FXR* and *SHP* double-knockout (DKO) mice displayed early-onset cholestasis, more severe liver damage, and higher BA synthesis than mice with loss of either gene alone (Anakk et al., 2011).

Ileum is the major site for BA reabsorption in the intestine (Baker and Searle, 1960; Buchwald and Gebhard, 1968; Thomas et al., 2008). BA/FXR signaling induces intestinal production of FGF15 (FGF19 in humans), which also inhibits *Cyp7a1* expression in hepatocytes by activating FGFR4 signaling (Fon Tacer et al., 2010; Inagaki et al., 2005). Selective *FXR* deletion or transgenic expression of an activated FXR in the intestine abolished or enhanced ileal *FGF15* expression (Modica et al., 2012; Stroeve et al., 2010). Recently, Diet1 was shown to be required for FGF15/19 expression in enterocytes (Vergnes et al., 2013). Gut microbiota, which metabolize primary BAs into secondary BAs, also regulate intestinal FGF15 production in an FXR-dependent manner (Sayin et al., 2013). Both *FGF15* and *FGFR4* KO mice exhibited elevated BA levels and enhanced *Cyp7a1* expression (Inagaki et al., 2005; Yu et al., 2000). Further, FXR agonist feeding failed to inhibit *Cyp7a1* expression in *FGFR4* or *FGF15* KO mice (Inagaki et al., 2005; Kong et al., 2012), suggesting that FGFR4 signaling is necessary for FXR-mediated repression of BA biosynthesis. Experimental data also showed that SHP was required for repression of *Cyp7a1* by exogenous FGF15/19 (Inagaki et al., 2005; Kir et al., 2012). SHP suppresses *Cyp7a1* expression via interaction with hepatocyte nuclear factor 4α

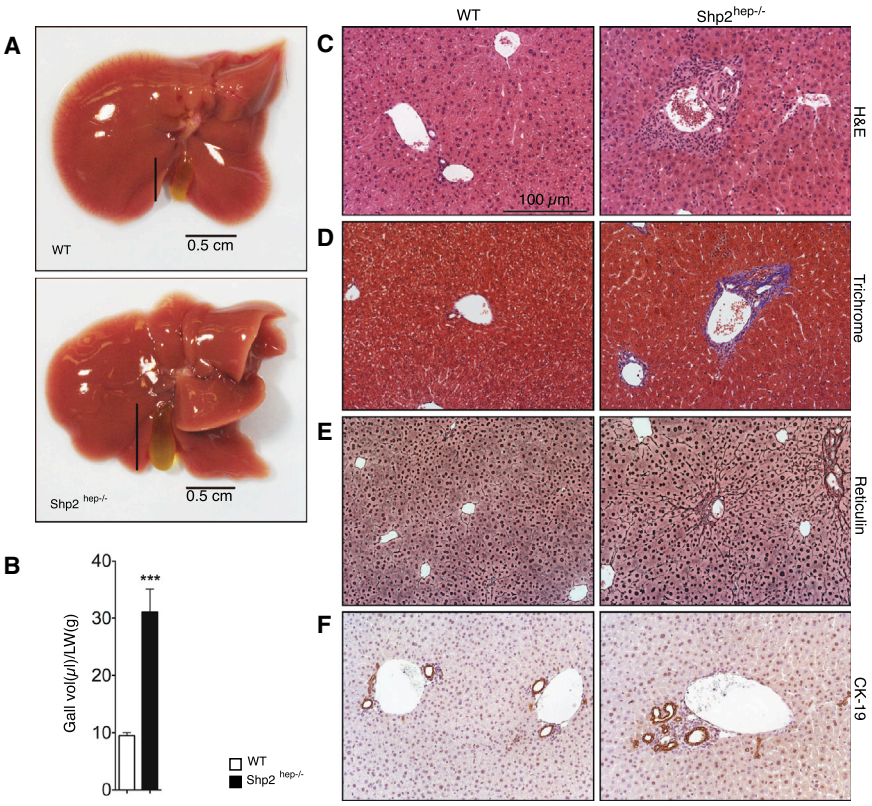

Figure 1. Hepatobiliary Defects in *Shp2*$^{hep-/-}$ Mice

(A) Macroscopic view of the whole livers from 2-month-old WT (*Alb-cre*$^{-}$*:Shp2*$^{fl/fl}$) and *Shp2*$^{hep-/-}$ (*Alb-cre*$^{+}$*:Shp2*$^{fl/fl}$) mice.

(B) Gallbladder volumes were adjusted by liver weight from WT and *Shp2*$^{hep-/-}$ mice (n = 6–7). Data are shown as mean ± SEM. ***p < 0.001.

(C–F) Liver sections were stained with H&E (C), Masson's Trichrome (D), reticulin (E), and CK-19 (F).

Scale bars in (D), (E) and (F) are the same as in (C).

(HNF4α) and liver receptor homolog-1 (LRH-1) on *Cyp7a1* promoter (Kir et al., 2012), both of which are regulators of *Cyp7a1* transcription (Inoue et al., 2006; Lu et al., 2000). Despite the dependence on SHP for transcriptional suppression of *Cyp7a1* by FGF19, no altered affinity to *Cyp7a1* promoter was detected for HNF4α, LRH-1, and SHP after FGF19 treatment (Kir et al., 2012). How activated FGFR4 signaling impacts on BA biosynthesis remains elusive.

Shp2 is a nonreceptor tyrosine phosphatase with two Src-homology 2 domains that promotes signaling through the Ras-Erk pathway (Chan and Feng, 2007; Neel et al., 2003). Mice with *Shp2/Ptpn11* ablated in hepatocytes (*Shp2*$^{hep-/-}$) displayed impaired hepatocyte proliferation and liver regeneration after partial hepatectomy (Bard-Chapeau et al., 2006). *Shp2*$^{hep-/-}$ animals suffered chronic hepatic injury and inflammation and were more susceptible to carcinogen-induced liver tumorigenesis (Bard-Chapeau et al., 2011). Here, we show that Shp2 loss in hepatocytes disrupts BA homeostasis and causes hepatobiliary damage. Our results identify Shp2 as a crucial factor that orchestrates the FGF15/19-FGFR4 and BA-FXR signaling pathways for control of BA biosynthesis.

RESULTS

Early-Onset Hepatobiliary Defects in Mice Deficient for Shp2 in Hepatocytes

In previous experiments, we generated a mouse line (*Shp2*$^{hep-/-}$, *Albumin-Cre*$^{+}$*:Shp2*$^{fl/fl}$) with Shp2 deleted in hepatocytes (Bard-Chapeau et al., 2006, 2011). We observed hepatic necrosis, inflammatory infiltration, and periportal fibrosis, dented lobe edges, and significantly enlarged gallbladders in *Shp2*$^{hep-/-}$ mice at the age of 2 months (Figures 1A–1D). These hepatic disorders are similar to those in rats fed with sodium cholate, a bile acid detergent (Jeong et al., 2005), or mice after bile duct ligation (BDL; Figure S1, available online) (Georgiev et al., 2008). Liver sections from *Shp2*$^{hep-/-}$ mice displayed evident biliary fibrosis around portal triad, with positive collagen staining (blue) around bile duct (Figure 1D). Stronger reticulin fiber staining (Figure 1E) also indicates hepatic damage in *Shp2*$^{hep-/-}$ mice. Around the portal triad, sporadic ductal cell proliferation was consistently observed in *Shp2*$^{hep-/-}$ livers, as revealed by cytokeratin-19 (CK-19) staining (Figure 1F). Together, these results demonstrate that ablating Shp2 in hepatocytes induces multiple hepatobiliary defects.

Shp2$^{hep-/-}$ Mice Are More Susceptible to BDL

The spontaneous hepatobiliary defects strongly suggest biliary dysfunction in *Shp2*$^{hep-/-}$ mice. To this end, we performed a BDL experiment, a well-characterized cholestasis model (Georgiev et al., 2008). Strikingly, almost all *Shp2*$^{hep-/-}$ mice (11/12) died within 4 weeks after BDL, while 75% of wild-type (WT) animals survived the experiment (Figure 2A). *Shp2*$^{hep-/-}$ mice displayed larger gallbladders 24 and 48 hr after surgery (Figures 2B and 2C) and more severe jaundice, with darker yellowish color seen on the palms (Figure 2D). Consistently, higher serum bilirubin and BA levels were detected in *Shp2*$^{hep-/-}$ than in WT mice at these time points (Figures 2D and 2E). However, *Shp2*$^{hep-/-}$ mice also exhibited decreasing serum BA levels from 24 to 48 hr after BDL (Figure 2E), and BDL induced larger areas of infarct in *Shp2*$^{hep-/-}$ mice as examined at 24 hr (Figure 2F). The more extensive necrosis and deteriorating liver function may explain the higher mortality and the drop in serum BA levels in *Shp2*$^{hep-/-}$ mice. Thus, the *Shp2*$^{hep-/-}$ mice were more vulnerable than WT controls to biliary obstruction, characterized by higher mortality rate, more severe liver damage, and jaundice.

Shp2 Deficiency in Hepatocytes Led to an Increase of Systemic BA Levels

We then measured BA levels in different ways. Consistent with the literature (Rao et al., 2008), WT female mice exhibited BA

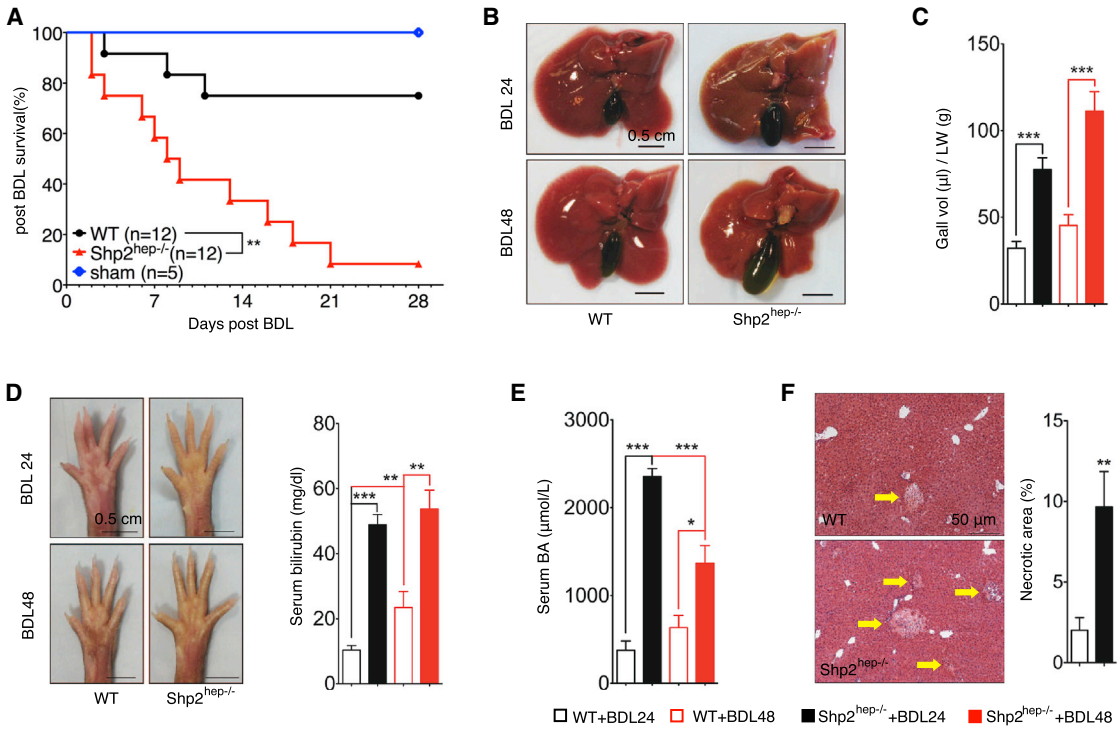

Figure 2. Severe Hepatobiliary Damages in *Shp2*$^{hep-/-}$ Mice following Bile Duct Ligation

(A) Kaplan-Meier survival analysis of WT and *Shp2*$^{hep-/-}$ mice after BDL. **p = 0.0014, as determined by log-rank (Mantel-Cox) test.

(B) Macroscopic views of WT and *Shp2*$^{hep-/-}$ livers were taken 24 and 48 hr after BDL.

(C) Gallbladder volumes were adjusted to liver weight after BDL (n = 4–10).

(D) Macroscopic view of palms was shown 24 and 48 hr after BDL. Serum bilirubin levels were measured (n = 6–12).

(E) Serum BA levels were measured after BDL (n = 6–12).

(F) Liver sections were stained with H&E (left), and statistical analysis (n = 5–7) of necrotic areas is shown to the right.

Data in (C), (D), (E), and (F) are shown as the mean ± SEM. **p < 0.01 and ***p < 0.001, as determined by Student's t test.

pool sizes larger than those of male mice (Figure 3A). The BA pool size increased significantly in both male and female *Shp2*$^{hep-/-}$ mice compared to controls (Figure 3A). Since an increase in BA pool size could be due to obstruction of bile flow or BA overproduction, we measured BA levels in serum, liver, gallbladder, and feces, as well as bile flow rate. Both hepatic and serum BA levels were elevated in *Shp2*$^{hep-/-}$ mice compared to controls (Figures 3B and 3F). Although the gallbladder BA concentrations were similar (Figure 3C), the total BA amounts in gallbladder were significantly elevated in *Shp2*$^{hep-/-}$ mice due to the larger size (Figures 1A and 1B). The bile flow rate in *Shp2*$^{hep-/-}$ mice increased significantly (Figure 3D), ruling out intrahepatic biliary obstruction. With similar weights of daily excretions of feces (Figure S2A), the daily fecal BA excretion was significantly higher in *Shp2*$^{hep-/-}$ than in control animals (Figure 3E). All of these results indicate elevation of systemic BA levels in *Shp2*$^{hep-/-}$ mice, which was evidently not caused by biliary hindrance.

Since different BA species may act as either FXR agonists or antagonists (Makishima et al., 1999; Parks et al., 1999; Sayin et al., 2013), we analyzed BA compositions in BA pool, liver, and feces. *Shp2*$^{hep-/-}$ mice exhibited a significant increase in relative fold (Figures 3G–3I, left panels) or absolute amounts (Figure S2B) for almost all BA species. The majority of BAs were conjugated in BA pool and liver (Figures 3G and 3H, middle and left panels), while most fecal BAs were unconjugated (Figure 3I, middle and left panels). The general representation of each species was similar in the BA pool and liver (Figures 3G and 3H, middle and left panels). Notably, the amount of FXR antagonist species tauro-β-muricholic acid (TβMCA) was unchanged in *Shp2*$^{hep-/-}$ liver, with a decrease in its representation in BA pools and feces (Figures 3G–3I). Further, the FXR agonist species, such as taurochenodeoxycholic acid (TCDCA), taurodeoxycholic acid (TDCA), taurolithocholic acid (TLCA), and taurocholic acid (TCA), increased significantly in the liver, and TLCA and TDCA even showed an increased representation in hepatic BA composition (Figure 3H).

BA Sequestration Ameliorates Hepatobiliary Defects in *Shp2*$^{hep-/-}$ Mice

Next, we asked whether the excess BAs are responsible for the hepatobiliary defects in *Shp2*$^{hep-/-}$ mice. We fed the mice with chow diet supplemented with 2% cholestyramine from weaning to 2 months old. Cholestyramine is a BA sequestrant that binds BAs to prevent its ileal reabsorption and to increase its fecal discharge, and therefore it lowers BA pool size in mice (Huang et al., 2006; Kong et al., 2012). The hepatobiliary defects including enlarged gallbladder, and dented edges were greatly

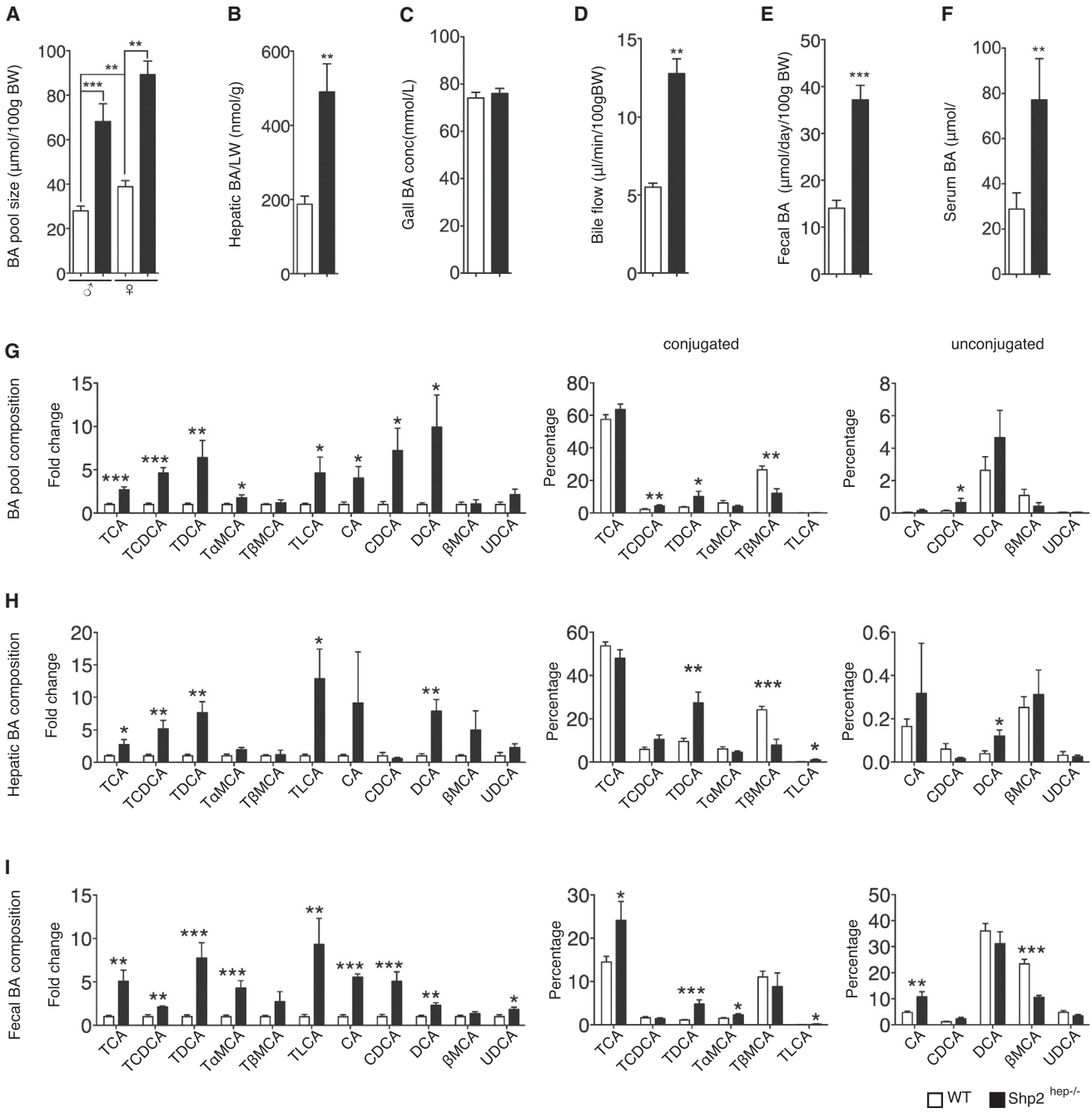

Figure 3. Elevation of Systemic BA Levels in *Shp2*$^{hep-/-}$ Mice

(A) BA pool (liver, gallbladder, and intestine) sizes were measured in both genders of the two genotypes (n = 6–10).

(B–E) BA levels in liver (B), gallbladder (C), feces (D), and serum (E) were measured (n = 5–11). All data were collected in males, hepatic BA concentration was adjusted to every gram of liver weight, and fecal BA excretion was adjusted to 100 g body weight/day.

(F) Bile flow rate was adjusted to 100 g body weight/min (n = 3).

(G–I) BA composition in BA pool (n = 6–9) (G), liver (n = 6–7) (H), and feces (n = 6–9) (I) was analyzed by liquid chromatography-mass spectrometry. The fold changes of BA species in *Shp2*$^{hep-/-}$ mice were calibrated to WT (the average value was designated as 1, left panels). The percentile representations of each conjugated and unconjugated BA species are shown in two panels separately in the right.

Data in (A)–(I) are shown as the mean ± SEM. *p < 0.05, **p < 0.01, and ***p < 0.001, as determined by Student's t test.

improved in *Shp2*$^{hep-/-}$ mice treated with cholestyramine (Figure 4A). Trichrome staining showed a significant decrease of portal fibrosis in *Shp2*$^{hep-/-}$ livers, down to the WT level (Figures 4B and 4E), with no obvious difference in reticulin staining (Figure 4C). Cholestyramine treatment reduced the liver/body weight ratios in WT and *Shp2*$^{hep-/-}$ mice (Figure 4D). Thus, these results

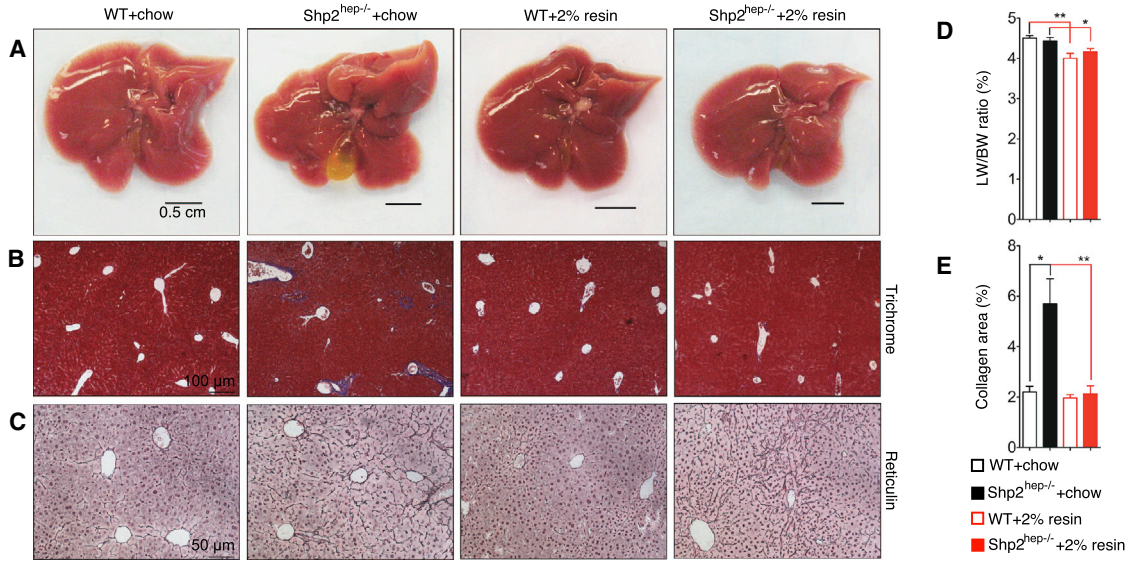

Figure 4. Lowering BA Levels in *Shp2*$^{hep-/-}$ Mice Alleviates Hepatobiliary Defects

(A) Macroscopic views of WT and *Shp2*$^{hep-/-}$ livers fed with chow without or with 2% cholestyramine from age of 3 weeks to 2 months.

(B) Liver sections were stained with Masson's Trichrome.

(C) Liver sections were stained with reticulin.

(D) The ratios of liver/body weight were determined for each group (n = 5–8).

(E) Collagen areas (blue) were measured from images in (B) (n = 4–7).

demonstrated that the hepatobiliary defects in *Shp2*$^{hep-/-}$ mice are, at least in part, due to the excess BAs.

BA Biosynthesis Is Dramatically Increased in *Shp2*$^{hep-/-}$ Liver

Without biliary obstruction, the augmented fecal BA excretion indicated a higher hepatic BA synthesis rate. Indeed, quantitative real-time PCR analysis revealed increased expression of key genes involved in both classical and alternative BA synthetic pathways (Chiang, 2002; de Aguiar Vallim et al., 2013), including *Cyp7a1*, *Cyp8b1*, and *Cyp27a1*, in *Shp2*$^{hep-/-}$ livers (Figure 5A). The increased *Cyp8b1* expression also explained the elevated TDCA levels in BA composition in *Shp2*$^{hep-/-}$ mice (Figures 3G–3I). Expression of the BA intoxication gene *Cyp3a11* was also increased in *Shp2*$^{hep-/-}$ livers (Figure 5A), likely due to increased hepatic BA levels. Similar to mRNA expression, elevated Cyp7a1 protein levels were detected in *Shp2*$^{hep-/-}$ livers (Figures 5B, S3A, and S3B). To determine if the elevated Cyp7a1 expression was caused by Shp2 ablation directly, we used another mouse model, *Mx1-Cre*$^{+}$*:Shp2*$^{fl/fl}$ (referred to as Shp$^{(H+K-/-)}$ hereafter), in which *Shp2* is acutely deleted in hepatocytes and nonparenchymal cells in adult mice following injection of polyinosinic:polycytidylic acid, poly(I:C) (Zhu et al., 2011). Consistently, acute removal of Shp2 also led to enhanced *Cyp7a1* expression significantly at both mRNA and protein levels (Figures 5C, 5D, and S3C). Therefore, the deregulated BA biosynthesis is a direct effect of Shp2 loss in hepatocytes. Consistent with previous reports (Huang et al., 2006; Kong et al., 2012), we found that the expression of both *Cyp7a1* and *Cyp8b1* markedly increased in WT mice after cholestyramine treatment (Figure 5E). Notably, cholestyramine feeding did not further increase *Cyp7a1* expression in *Shp2*$^{hep-/-}$ livers, but it had an enhancing effect on *Cyp8b1* (Figure 5E). Immunoblot analysis confirmed the quantitative real-time PCR result on *Cyp7a1* expression in WT and *Shp2*$^{hep-/-}$ livers (Figures 5F and S3D). Cholestyramine treatment induced modest reduction of *SHP* expression in WT and further decreased *SHP* expression in *Shp2*$^{hep-/-}$ livers (Figure 5E).

The basal *SHP* expression was significantly downregulated in *Shp2*$^{hep-/-}$ livers (Figures 5A and 5E). Given the elevated FXR agonist BA species and unchanged antagonist TβMCA in *Shp2*$^{hep-/-}$ livers, decreased *SHP* expression suggests defective FXR signaling. To address this, we first examined FXR protein expression and subcellular distribution. Cytoplasmic and nuclear fractions were prepared, and immunoblotting showed clean separation of the two fractions using HSP90 as the cytoplasmic marker and lamin B1 for nucleus (Figure 5G). Deletion of Shp2 did not alter FXR protein level or its nuclear localization (Figure 5G). Notably, Shp2 was almost exclusively located in the cytoplasm (Figure 5G), and we failed to detect physical association of Shp2 with FXR even with overexpressed tagged FXR by coimmunoprecipitation (data not shown). By chromatin immunoprecipitation (ChIP) assay, we found that binding of FXR to the *SHP* promoter was unchanged in *Shp2*$^{hep-/-}$ livers (Figure 5H).

To further determine the FXR activation status, we fed both WT and *Shp2*$^{hep-/-}$ mice with synthetic FXR agonist GW4064 by oral gavage. Hepatic *SHP* expression was significantly induced in WT mice, but no *SHP* induction was observed in *Shp2*$^{hep-/-}$ mice (Figure S3E). However, GW4064 induced *SHP* expression in the ileums of both WT and *Shp2*$^{hep-/-}$ mice, where Shp2 expression was intact (Figure S3E). This result strongly suggests defective FXR activation in Shp2-deficient hepatocytes. We also examined HNF4α and LRH-1, two nuclear receptors that bind and activate *Cyp7a1* promoter (Kir et al., 2012; Lu et al., 2000).

Both mRNA and protein levels of HNF4α and LRH-1 remained unchanged in *Shp2*$^{hep-/-}$ liver (Figures 5A and 5G). Similar binding of HNF4α and LRH-1 to *Cyp7a1* promoter was detected by ChIP in WT and *Shp2*$^{hep-/-}$ livers (Figures 5I and 5J).

To determine if the BA overproduction is fueled by excess cholesterol in mutant mice, we measured cholesterol levels in serum, liver, and gallbladder. Serum cholesterol was even lower in *Shp2*$^{hep-/-}$ than in WT mice (Figure 5M), while the cholesterol concentrations in liver (Figure 5N) and gallbladder (Figure 5O) were similar. Notably, the expression of cholesterol synthesis-related genes, such as *HMGCR* and *ACAT2*, was enhanced in *Shp2*$^{hep-/-}$ livers (Figure 5P). Thus, aberrantly increased BA synthesis in *Shp2*$^{hep-/-}$ livers lowered circulating cholesterol levels, resulting in a compensatory increase of hepatic cholesterol synthesis.

Shp2 Mediates Both FGF15/19 and BA Signals to Suppress BA Synthesis

Given the elevated bile flow and enhanced fecal excretion of BAs in *Shp2*$^{hep-/-}$ animals (Figure 3), we measured ileal expression of *FGF15* and *SHP*, both of which are induced by ileal BA-FXR signaling (Kong et al., 2012; Modica et al., 2012; Stroeve et al., 2010). The mRNA levels of *FGF15* and *SHP* were markedly increased in the ileum of mutant mice (Figure 6A), in which Shp2 expression was normal (Figure S4A). The failed repression of BA synthesis in the mutant liver and the drastically elevated ileal *FGF15* expression suggests insensitivity of Shp2-deficient hepatocytes to this gut hormone. To test this, we injected recombinant hFGF19 intraperitoneally (i.p.) and measured gene expression 6 hr later. Exogenous hFGF19 exerted a strong inhibition of *Cyp7a1* and *Cyp8b1* expression in WT controls (Figures 6B, 6C, and S4B). However, the response of *Shp2*$^{hep-/-}$ livers to hFGF19 was significantly diminished (though not completely blocked), as evaluated by Cyp7a1 mRNA and protein levels (Figures 6B, 6C, and S4B). Furthermore, hFGF19 failed to upregulate *SHP* expression in *Shp2*$^{hep-/-}$ livers (Figure 6B).

To identify Shp2-modulated signaling events downstream of FGFR4, receptor for FGF15/19, we prepared liver lysates 30 min after hFGF19 injection. hFGF19 potently stimulated Erk1/2 phosphorylation in WT, but not in *Shp2*$^{hep-/-}$ livers (Figures 6D and S4C), and similarly, defective activation was also observed for ribosomal S6 kinase (p90RSK) (Figure 6D). The specific effect on Erk1/2 activation by hFGF19 was ascertained by the similar p-p38 MAPK levels detected in both lysates (Figures 6D and S4C). In contrast, FGF19-induced p-Jnk signals were higher in *Shp2*$^{hep-/-}$ liver (Figures 6D and S4C), consistent with our previous observations (Bard-Chapeau et al., 2006; Shi et al., 1998). Using an antibody that recognizes several protein kinase C (PKC) family members, we detected hFGF19-induced phosphorylation of PKCs in controls, which was attenuated in *Shp2*$^{hep-/-}$ livers (Figures 6D and S4C). To rule out the effect by the chronic liver damages in *Shp2*$^{hep-/-}$ mice, we injected hFGF19 into Shp2$^{(H+K)-/-}$ mice and obtained similar results in these mice (Figure S4D). All of these data suggest that Shp2 deletion suppressed hFGF19-stimulated Erk and PKC activation in hepatocytes.

With the reduced response to FGF15/19 signal, the elevated BA levels failed to activate FXR to upregulate *SHP* expression in *Shp2*$^{hep-/-}$ livers, suggesting a role of Shp2 upstream of FXR. To test this, we investigated if expression of a constitutively active FXR can rescue Shp2 deficiency and therefore inhibit *Cyp7a1* expression. Adenoviruses expressing VP16-FXR, SHP, or VP16 were injected into WT and *Shp2*$^{hep-/-}$ mice through tail vein. Similarly, increased *SHP* expression was observed in both WT and *Shp2*$^{hep-/-}$ livers after VP16-FXR injection (Figure 6E). *Cyp7a1* mRNA and protein levels were decreased in WT livers and were also downregulated to a lesser extent in *Shp2*$^{hep-/-}$ livers (Figures 6E, 6F, and S4E). *SHP* overexpression also suppressed Cyp7a1 expression in *Shp2*$^{hep-/-}$ livers, though not to the level of WT (Figures 6E, 6F, and S4E). These results argue that FXR and SHP do not operate in a simple linear relationship and also suggest that Shp2 modulates signaling to both independently. Although *Cyp8b1* expression was significantly elevated in *Shp2*$^{hep-/-}$ livers (Figures 5A and 6E), overexpression of VP16-FXR or SHP caused similar suppression of *Cyp8b1* in control and mutant mice (Figure 6E). Thus, the expression of *Cyp7a1* and *Cyp8b1* is likely controlled by common and distinct pathways.

Shp2 Is Required for Hepatic FGFR4 Activation by FGF15/19

As described above, Shp2 is required for hepatic response to ileal FGF15/19 signal and also for intrahepatic FXR activation by BAs. To gain a broad view on Shp2 function, we performed microarray analysis of gene expression in 2-month-old *Shp2*$^{hep-/-}$ and WT livers and compared the results with two published data sets. One was on FGF15/19-treated livers (Potthoff et al., 2011) that showed induction of Erk pathway and inhibition of BA synthesis. Another was on *FXR/SHP* DKO livers that exhibited increased BA synthesis (Anakk et al., 2011). Overall, opposite gene expression patterns were observed between *Shp2*$^{hep-/-}$ and FGF15/19-treated livers (Figure S5A). Only one group of upregulated genes is enriched between *Shp2*$^{hep-/-}$ and FXR/SHP DKO mice (Figure S5A). Gene ontology (GO) analysis showed significant enrichment of BA metabolism-related processes, such as steroid synthesis and primary BA biosynthesis, in the group of upregulated genes in *Shp2*$^{hep-/-}$ livers, which were downregulated in FGF15/19-treated livers (Figure S5B). Furthermore, GO analysis revealed a group of genes that were upregulated in both *Shp2*$^{hep-/-}$ and *FXR/SHP* DKO livers and also a set of genes that were oppositely regulated in FGF15/19-treated and *FXR/SHP* DKO livers (Figure S5B). Therefore, the large-scale data analysis suggests that Shp2 is a positive regulator of FGF15/19 signal and acts cooperatively with FXR and SHP in hepatic control of BA synthesis.

We further dissected the effect of Shp2 deficiency on signaling events proximal to FGFR4. Treatment of Hep3B cells with hFGF19 induced robust tyrosine-phosphorylation of FGFR4 and its immediate target FRS2α (Figures 7A and 7B). Consistent with a previous report (Zhou et al., 2009), FRS2α was also highly phosphorylated at serine/threonine residues (Figure 7B). hFGF19 stimulation induced physical association of FGFR4 with FRS2α (Figure 7A) and assembly of Shp2/FRS2α and Shp2/Gab1 complexes (Figures 7C and 7D). shRNA-mediated Shp2 knockdown (KD) decreased tyrosyl phosphorylation of FGFR4 (Figure 7E) and reduced FRS2α phosphorylation on tyrosine and serine (Figure 7F), resulting in impaired Erk activation (Figures 7E and 7F).

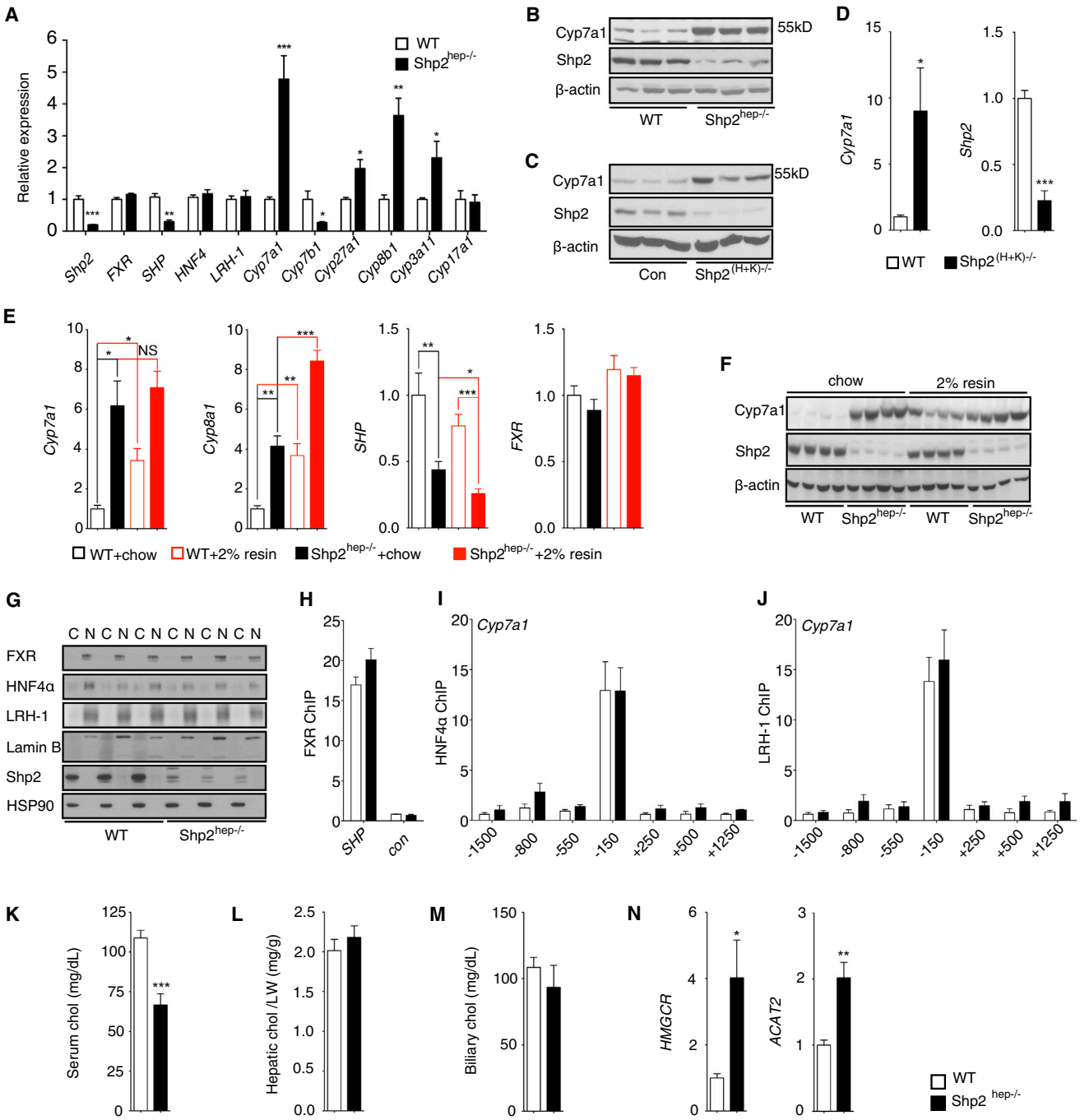

Figure 5. BA Synthesis-Related Genes Are Significantly Upregulated in *Shp2*$^{hep-/-}$ Liver

(A) The expression of genes as indicated was determined by quantitative real-time PCR in 2-month-old WT or *Shp2*$^{hep-/-}$ livers (n = 4–5).

(B) Cyp7a1, Shp2, and β-actin protein levels were determined by immunoblotting of liver lysates from WT and *Shp2*$^{hep-/-}$ mice. Each lane represents each mouse.

(C) Cyp7a1, Shp2, and β-actin protein levels were determined by immunoblotting liver lysates from control and *Shp2*$^{(H+K)-/-}$ mice. Each lane represents each mouse.

(D) Relative expression of *Shp2* and *Cyp7a1* was measured by quantitative real-time PCR in liver extracts of WT and *Shp2*$^{(H+K)-/-}$ mice following poly(I:C) injection (n = 5).

(E) Hepatic expression of *Cyp7a1*, *Cyp8b1*, *SHP*, and *FXR* mRNAs was determined by quantitative real-time PCR in mice fed with chow without or with 2% cholestyramine from 3 weeks to 2 months (n = 4–8).

(F) Cyp7a1, Shp2, and β-actin protein levels were determined by immunoblotting liver lysates as in (F). Each lane represents each mouse.

(G) Cytoplasmic (C) and nuclear (N) fractions were prepared from freshly isolated liver samples. FXR, HNF4α, LRH-1, Lamin B (nuclear marker), Shp2, and Hsp90 (cytoplasmic marker) protein levels were determined by immunoblot analysis. Each pair of C and N samples was prepared from the same mouse.

(legend continued on next page)

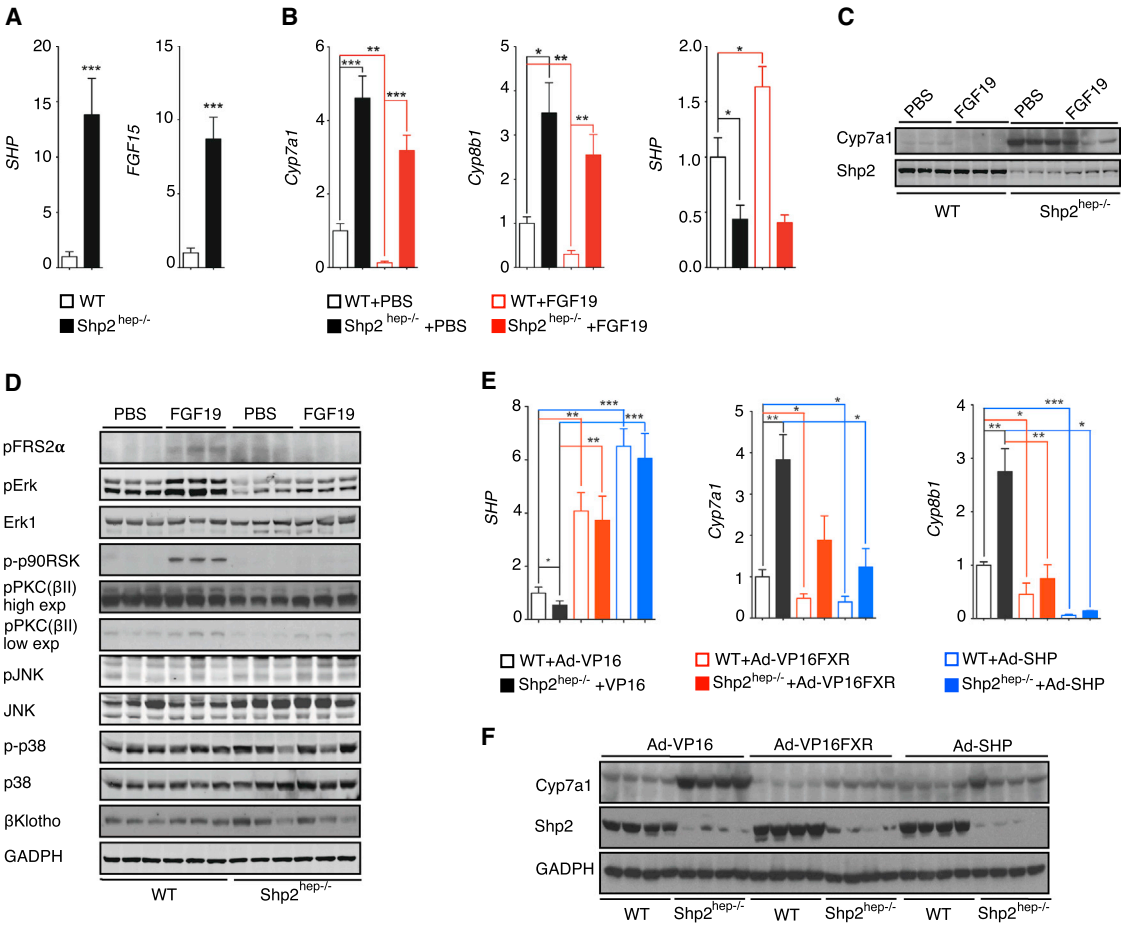

Figure 6. *Shp2*$^{hep-/-}$ Mice Are Refractory to FGF15/19 Repression of BA Synthesis

(A) Relative expression of *SHP* and *FGF15* mRNA was determined by quantitative real-time PCR in ileum samples (n = 5–7).

(B) Relative expression of *Cyp7a1*, *Cyp8b1*, and *SHP* mRNAs in liver samples was determined by quantitative real-time PCR. The animals (n = 5–10) were injected with PBS or hFGF19 (1 mg/kg body weight) and fasted for 6 hr before sample collection.

(C) Cyp7a1 and Shp2 protein levels were determined by immunoblot analysis of liver lysates from mice as in (B). Each lane represents one mouse.

(D) Immunoblotting of liver lysates was performed with antibodies against pFRS2α(Y196), pErk, Erk1, p-p90RSK, p-PKC(pan) (βII Ser660), pJNK, JNK, p-p38, p38, β-Klotho, and GAPDH. WT or *Shp2*$^{hep-/-}$ mice (2 months old) were fasted for 5.5 hr before i.p. injection of PBS or hFGF19 (1 mg/kg body weight). The animals were sacrificed 30 min after injection.

(E) Relative expression of *SHP*, *Cyp7a1*, and *Cyp8b1* mRNA was determined by quantitative real-time PCR in liver samples. The mice (n = 4–5) were injected with 2×10^9 virions of VP16, VP16-FXR, or SHP adenoviruses through tail vein, and liver samples were collected 5 days later.

(F) Cyp7a1, V5, Shp2, and GAPDH protein levels were determined by immunoblotting liver samples collected as in (E). Each lane represents one mouse.

Relative gene expression was normalized to *β-actin*, and fold change was calibrated to the WT group. Data are shown as the means ± SEM. *p < 0.05, **p < 0.01, and ***p < 0.001 as determined by Student's t test.

Consistent with the observations in Hep3B cells, FRS2α was not phosphorylated in *Shp2*$^{hep-/-}$ liver following hFGF19 injection, suggesting defective FGFR4 activation (Figure 6D). However, *FGFR4* mRNA levels remained unchanged in mutant livers and were not affected by hFGF19 injection (Figure S5D). Treatment with hFGF19 for 6 hr induced downregulation of FGFR4 in WT livers (Figures 7H and S5C), suggesting that activation of FGFR4 is followed by endocytosis and degradation after ligand

(H) ChIP was performed with liver samples (n = 3) using FXR antibody. qPCR was performed with the FXR binding region on *SHP* promoter (*SHP*) and coding region (*con*). Data are shown as fold enrichment.

(I and J) ChIP assay was performed with HNF4α (I) or LRH-1 (J) antibodies and different DNA sequences in *Cyp7a1* promoter and proximal regions (n = 4). Data are shown as fold enrichment.

(K–M) Cholesterol (chol) levels of serum (K), liver (L), and gallbladder (M) were measured. Hepatic cholesterol was adjusted to mg/liver weight (L).

(N) Hepatic expression of *HMGCR and ACAT2* mRNA was determined by quantitative real-time PCR (n = 4–5).

All PCR data were normalized against *β-actin*, and fold change was calibrated to the WT group. Data (in A, D, E, and H–N) are shown as the means ± SEM. *p < 0.05, **p < 0.01, and ***p < 0.001 as determined by Student's t test.

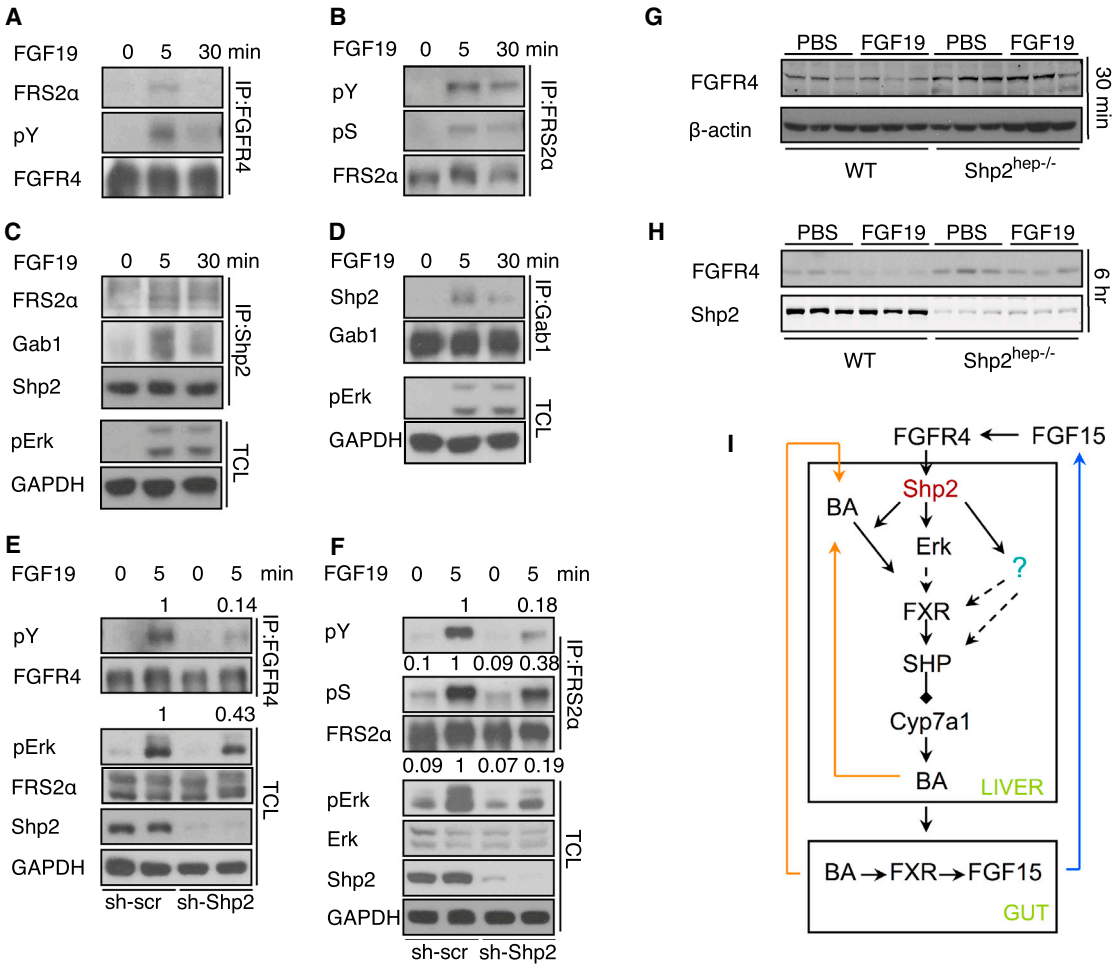

Figure 7. Shp2 Is Required for FGF15/19-Stimulated FGFR4 Activation

(A–F) Serum-starved Hep3B cells were stimulated with 100 ng/ml hFGF19 as indicated. (A) Cell lysates were subjected to immunoprecipitation with anti-FGFR4 antibody and then immunoblotted with FRS2α, pY, or FGFR4 antibodies. (B) Immunoprecipitates of anti-FRS2α antibody were immunoblotted against pY, pS, or FRS2α antibodies. (C) Immunoprecipitates of anti-FRS2α antibody were immunoblotted with FRS2α, Gab1, or Shp2 antibodies, and immunoblotting was also performed with total cell lysate (TCL) against pErk and GAPDH. (D) Immunoprecipitates by Gab1 were immunoblotted against Shp2 or Gab1 antibodies, and TCLs were also immunoblotted with antibodies to pErk or GAPDH. In (E) and (F), the cells were treated with lentiviruses expressing either scrambled (sh-scr) or Shp2-specific (sh-Shp2) shRNAs for 72 hr before starvation. (E) Immunoblotting was performed with anti-FGFR4 immunoprecipitates using antibodies to pY or FGFR4, and TCL was also immunoblotted with antibodies as indicated. (F) Immunoblotting was performed for anti-FRS2α immunoprecipitates using pY, pS, or FRS2α antibodies, and also with TCL using antibodies as indicated.

(G) The same samples as in Figure 6D were blotted with antibodies to FGFR4 and β-actin.

(H) The same samples as in Figure 6C were immunoblotted for FGFR4 and Shp2.

(I) A model shows how Shp2 orchestrates BA and FGF15/19 signaling in the control of BA biosynthesis.

binding, similar to other FGFRs reported previously (Beenken and Mohammadi, 2009; Haugsten et al., 2008). Notably, this process was attenuated in *Shp2*$^{hep-/-}$ livers, as evidenced by more steady FGFR4 protein contents after hFGF19 treatment (Figures 7G, 7H, and S5C). These results indicate a requirement of Shp2 for FGF15/19 activation of FGFR4 and its downstream signaling pathways in hepatocytes.

DISCUSSION

Tight control of BA homeostasis is essential, given the critical roles of BAs in lipid digestion and cholesterol metabolism as well as the toxic effect of excess BAs. Numerous data suggested crosstalk of FGF15/19-FGFR4 and BA-FXR signaling events, although the underlying mechanism is unclear. This report presents physiological and biochemical data proving that Shp2 acts to coordinate the signals elicited by FGF15/19 and BAs in the liver (Figure 7I).

The *Shp2*$^{hep-/-}$ mice exhibited early-onset hepatobiliary defects, including enlarged gallbladder, elevation of systemic BA levels, and ductal cell proliferation (Figures 1 and 3). Furthermore, *Shp2*$^{hep-/-}$ animals were more susceptible to biliary obstruction (Figure 2). BA sequestration by cholestyramine improved the hepatobiliary phenotypes (Figure 4), suggesting that excess BAs account for the liver damages. The increased fecal BA discharge, together with elevated bile flow (Figures

3D and 3E), directly points to unrestrained BA synthesis in *Shp2*$^{hep-/-}$ mice. Indeed, several lines of evidence highlight an indispensable role of Shp2 in repression of BA synthesis. First, basal levels of *Cyp7a1* mRNA and protein were markedly increased in *Shp2*$^{hep-/-}$ livers (Figure 5). Second, increased intrahepatic BAs did not suppress BA synthesis in Shp2$^{-/-}$ hepatocytes (Figures 5 and 6). Third, increased ileal FGF15 expression, and even i.p. injection of hFGF19, did not effectively inhibit BA synthesis in mutant mice (Figures 6A–6D). These observations indicate that Shp2 is positively required for hepatic response to both intrahepatic and ileal inhibitory signals.

It has been well recognized that the BA-FXR-SHP axis plays a central role in repression of *Cyp7a1* expression. However, phenotypic analyses of *FXR* and *SHP* KO or DKO mice argued against a simple linear relationship of the FXR-SHP-*Cyp7a1* pathway (Anakk et al., 2011; Sinal et al., 2000). Our results indicate defective FXR activation in *Shp2*$^{hep-/-}$ livers. First, the BA composition analysis showed an increase of most FXR agonist species with similar levels of antagonist in *Shp2*$^{hep-/-}$ livers (Figures 3G–3I). However, the basal *SHP* expression was reduced in the mutant livers (Figure 5A). Second, synthetic FXR agonist GW4064 failed to upregulate *SHP* expression in *Shp2*$^{hep-/-}$ livers (Figure S3E). Third, exogenous expression of an activated FXR or SHP partially repressed Cyp7a1 expression (Figure 6), placing Shp2 upstream of FXR. However, with distinct subcellular localization (Figure 5G), Shp2 does not form a physical complex with and regulate FXR activity directly.

The defective response to hFGF19 in *Shp2*$^{hep-/-}$ livers is very similar to that of *FGFR4* and *FGF15* KO mice, indicating a critical role of Shp2 in this pathway. With normal expression of Shp2 in the ileum (Figure S4A), the intestinal BA-FXR signaling remained intact in *Shp2*$^{hep-/-}$ animals. In fact, ileal *FGF15* and *SHP* expression was increased (Figure 6A) due to enhanced bile flow. However, this data may have also revealed a compensatory mechanism for the insensitivity of Shp2$^{-/-}$ hepatocytes to FGF15. Indeed, i.p. injection of hFGF19 suppressed *Cyp7a1* and *Cyp8b1* expression in WT livers, but this response was diminished in *Shp2*$^{hep-/-}$ livers (Figure 6). Tyrosyl phosphorylation of FGFR4 and FRS2α was reduced in Shp2 KD cells following hFGF19 stimulation (Figure 7E). The ligand-stimulated FGFR4 activation/downregulation was also attenuated in *Shp2*$^{hep-/-}$ livers (Figures 7G and 7H). These biochemical data suggest a requirement for Shp2 in FGFR4 activation by hFGF19, which involves its association with FRS2α.

Consistently, we detected multiple signaling defects downstream of FGFR4 in *Shp2*$^{hep-/-}$ livers and Shp2 KD cells. hFGF19-stimulated p-Erk1/2 and p90RSK activation was almost blocked in *Shp2*$^{hep-/-}$ livers (Figure 6D). Consistently, several groups reported that pharmaceutical- or siRNA-mediated inhibition of Erk alleviated repression of *Cyp7a1* expression in human hepatocytes or mouse livers (Henkel et al., 2011; Li et al., 2012b; Song et al., 2009). Therefore, defective Erk activation may account for deregulated BA synthesis in Shp2$^{-/-}$ hepatocytes. Several molecules have been proposed as potential Shp2 targets in promoting the Erk pathway, including PAG/Cbp, RasGAP, Gab1, and Sprouty (Chan and Feng, 2007; Neel et al., 2003). Previous data also suggested BA activation of PKCα, PKSβ, and PKCδ (Gineste et al., 2008; Rao et al., 1997), and a recent report showed PKCζ activation by FGF19 (Seok et al., 2013). These studies suggested a mechanism for FXR regulation via phosphorylation by PKCs, which can be stimulated by FGF15/19. We observed that Shp2 deficiency resulted in reduced PKC phosphorylation in control and hFGF19-treated livers. Further studies are needed to elucidate distinct roles of specific PKC isoforms in FGFR4 signaling and FXR activation. Together, our results show that Shp2 is a critical player immediately downstream of FGFR4 to regulate BA synthesis. The biochemical data were further supported by comparative analysis of global gene expression profiles in Shp2$^{hep-/-}$, *FXR*/*SHP* DKO and FGF15/19-treated livers (Figures S5A and S5B).

BAs are also considered as carcinogens due to their amphipathic nature (Wang et al., 2013). Both *FXR* and *SHP* KO animals developed liver cancers spontaneously (Yang et al., 2007; Zhang et al., 2008). *FXR*/*SHP* DKO mice suffered from accelerated liver tumorigenesis due to BA activation of Hippo signaling (Anakk et al., 2013). *Shp2*$^{hep-/-}$ mice developed hepatocellular adenomas spontaneously and were more susceptible to chemical carcinogen (Bard-Chapeau et al., 2011; Li et al., 2012a). Lowering BAs by cholestyramine significantly improved hepatobiliary damages in mutant animals, suggesting that persistent elevation of hepatic BA contents is a contributing factor to oncogenesis in Shp2-deficient livers. Recent studies showed that *FGF19* and *FGFR4* are deregulated in several human cancers (Desnoyers et al., 2008; French et al., 2012). In *Shp2*$^{hep-/-}$ mice, upregulated ileal *FGF15* expression (Figure 6A) may contribute to enhanced liver tumorigenesis.

BA biosynthesis is a primary route for disposal of excess cholesterol, and the intricate balance between BAs and cholesterol is exemplified by the cholesterol-lowering effect of BA sequestration. Similar to *Cyp7a1* transgenic mice (Li et al., 2011), *Shp2*$^{hep-/-}$ animals also showed lower plasma cholesterol levels and increased hepatic cholesterol synthesis (Figures 5M and 5P), indicating that the enhanced BA synthesis is not driven by cholesterol accumulation but rather is due to uncontrolled expression of *Cyp7a1* and other BA synthetic genes. All this supports Shp2 as a bona fide regulator of BA biosynthesis.

EXPERIMENTAL PROCEDURES

Animal Procedures

Generation of hepatocyte-specific Shp2 KO mice (*Shp2*$^{hep-/-}$) were described previously (Bard-Chapeau et al., 2011; Bard-Chapeau et al., 2006). The animal protocols (S09108) with all used procedures were approved by the UCSD Institutional Animal Care and Use Committee. BDL was performed as previously reported (Georgiev et al., 2008). For BA sequestration, mice were fed with chow diet (Cat. No. 7012, Harlan Laboratories) supplemented with 2% cholestyramine-resin (Cat. No. C4650, Sigma-Aldrich) from weaning to 2 months. All experimental data were collected from male animals at the age of 8–10 weeks, except that BDL and measurement of BA pool size and bile flow were done on both male and female mice. All samples were collected from WT and mutant animals between 3:00 and 5:00 p.m. during the day.

Histology Staining and Image Acquisition

Liver samples were prepared as reported (Bard-Chapeau et al., 2011), embedded, sectioned, and stained with hematoxylin and eosin (H&E) at a UCSD core facility. Masson's Trichrome Staining (Cat. No. KTMTRPT, American MasterTech) and reticulin staining (Cat. No. KTCPRPT, American MasterTech) were performed following the manufacturer's instructions. Necrotic areas were counted using ImageJ and normalized with parenchymal areas. The images were acquired with an Olympus IX71 microscope and CellSense Software.

Quantitative Real-Time PCR and Immunoblot Analyses

Liver or ileum samples were lysed in TRIzol reagent (Cat. No. 15596, Invitrogen) using MagNA Lyser (Roche). RNA was extracted and reverse transcribed with a kit (Cat. No. 4374966, Invitrogen). Quantitative real-time PCR was performed with commercial master mix (Cat. No. 600882, Agilent Technologies) using Mx3000P QPCR system (Agilent Technologies). A list of PCR primers is provided in the Supplemental Information. Immunoblot analysis was performed with standard protocols and visualized with ECL or ECL plus. Some blots were visualized by LI-COR Odyssey system. The list of primary antibodies is provided in the Supplemental Information. Freshly isolated liver lysates were separated into cytoplasmic and nuclear fractions using a kit (Pierce, Cat. No. 78835).

Measurement of BAs, Bilirubin, and Cholesterol

Bile flow rate was measured as described previously (Modica et al., 2011). Levels of total bile acids (Cat. No. DZ042A-K, Diazyme), total bilirubin (Cat. No. B577, Teco Diagnostics), and total cholesterol (Cat. No. 439-17501, Wako Diagnostics) were measured according to the manufacturer's instructions. BA composition in BA pool, liver, and feces was analyzed as previously reported (Li et al., 2012b).

Cell Culture, Treatment, and Immunoprecipitation

Hep3B cells (ATCC HB-8064) were starved in Dulbecco's modified Eagle's medium (DMEM) with 1% fetal bovine serum (FBS) for 16 hr and stimulated with 100 ng/ml hFGF19 in DMEM for the indicated time periods. Immunoprecipitation was performed as reported (Shi et al., 2000). Tyrosyl-phosphorylated proteins were detected with three anti-pY antibodies combined (Supplemental Information).

Adenovirus and Lentivirus Generation and Purification

PCR fragments of *VP16*, *VP16-FXR*, and *SHP* were cloned into pENTR/D-TOPO and then shuttled into pAd/CMV/V5-DEST. *VP16-FXR* fragment was amplified with *VP16-ad-F* and *FXR-ad-R* primers. The virus stocks were generated according to the manufacturer's instructions. The purification and titration of viruses were performed as previously described (Qiao et al., 2006). Lentivirus constructs with scrambled or Shp2-specific shRNAs were generated as previously reported (Lu et al., 2011).

Microarray and Bioinformatic Data Analysis

Total RNA from $Shp2^{hep-/-}$ and WT mice liver was prepared with RNeasy Mini Kit (QIAGEN Cat. No. 74104). Labeled cRNA was prepared from 500 ng RNA using the Illumina RNA Amplification Kit from Ambion. The labeled cRNA (750 ng) was hybridized overnight at 58°C to the Sentrix Mouse-8 Expression BeadChip (>23,000 gene transcripts; Illumina) according to the manufacturer's instructions. BeadChips were subsequently washed and developed with fluorolink streptavidin-Cy3 (GE Healthcare). BeadChips were scanned with an Illumina BeadArray Reader.

The gene expression data (GSE20599) for $FXR^{-/-}/SHP^{-/-}$ DKO mice at 5 weeks of age were downloaded from the GEO (Anakk et al., 2011), processed with BeadStudio software, and quantile normalized. The data (GSE29426) for FGF15/19-treated mice were downloaded from GEO (Potthoff et al., 2011) and processed with MAS5 algorithm (Affymetrix). Probes were filtered with detection p value > 0.01 (for $Shp2^{hep-/-}$ and $FXR^{-/-}/SHP^{-/-}$ DKO data) or with ABS call (for FGF15/19 data) before further analysis. Transcripts shared between data sets were used for K-means clustering with Cluster 3.0 software. Heatmaps were generated with Java TreeView. GO analysis was performed with DAVID v.6.7 program.

Statistical Analyses

Data analysis was performed using a two-tailed unpaired Student's t test. Values are expressed as mean ± SEM (*$p < 0.05$; **$p < 0.01$; ***$p < 0.001$).

ACCESSION NUMBERS

The microarray data have been deposited in the Gene Expression Omnibus (GEO) under the accession number GSE51860.

SUPPLEMENTAL INFORMATION

Supplemental Information includes Supplemental Experimental Procedures, five figures, and three tables and can be found with this article online at http://dx.doi.org/10.1016/j.cmet.2014.05.020.

AUTHOR CONTRIBUTIONS

S.L. and G.-S.F. conceived the project, analyzed the data, and wrote the paper. G.-S.F. provided the reagents. S.L. designed and performed most of the experiments. D.D.F.H. did the BA measurements and made FXR and VP-16 FXR virus stocks. X.L. provided some animals and microarray data. S.L., N.A., and L.Q. purified the adenoviruses. N.A. performed the liver fraction and some western blots. J.L. made the SHP adenovirus stock. L.M. helped set up the ChIP assay. H.H.Z. provided liver samples from $Shp2^{H+K-/-}$ mice, and J.S. and Z.H. helped design the experiments and analyzed the data. T.L. performed the BA composition analysis. B.L. performed the bioinformatics analysis. K.S.-P. and H.E.X. prepared recombinant hFGF19, and K.J. did the histology analysis.

ACKNOWLEDGMENTS

We thank R. Evans (Salk Institute) for the vp16-FXR construct, J. Luo (Peking University) for the Shp2 knockdown lentiviruses, Z. Chen (Shanghai Institute of Biochemistry and Cell Biology) for anti-FRS2α antibody, and J. Qi (University of Maryland) and G. Hon (UCSD) for helpful discussion and protocols. This research was supported by NIH grants R01HL096125 and R01CA176012 (G.S.F.), R01DK066202 (H.E.X.), R01HD069634 (J.S.), and P20GM103549 (T.L.) and ADA grant 1-13-BS-048 (G.S.F.). The authors declare no competing financial interests.

Received: December 12, 2013
Revised: April 18, 2014
Accepted: May 16, 2014
Published: June 26, 2014

REFERENCES

Anakk, S., Watanabe, M., Ochsner, S.A., McKenna, N.J., Finegold, M.J., and Moore, D.D. (2011). Combined deletion of Fxr and Shp in mice induces Cyp17a1 and results in juvenile onset cholestasis. J. Clin. Invest. *121*, 86–95.

Anakk, S., Bhosale, M., Schmidt, V.A., Johnson, R.L., Finegold, M.J., and Moore, D.D. (2013). Bile acids activate YAP to promote liver carcinogenesis. Cell Rep *5*, 1060–1069.

Baker, R.D., and Searle, G.W. (1960). Bile salt absorption at various levels of rat small intenstine. Proc. Soc. Exp. Biol. Med. *105*, 521–523.

Bard-Chapeau, E.A., Yuan, J., Droin, N., Long, S., Zhang, E.E., Nguyen, T.V., and Feng, G.S. (2006). Concerted functions of Gab1 and Shp2 in liver regeneration and hepatoprotection. Mol. Cell. Biol. *26*, 4664–4674.

Bard-Chapeau, E.A., Li, S., Ding, J., Zhang, S.S., Zhu, H.H., Princen, F., Fang, D.D., Han, T., Bailly-Maitre, B., Poli, V., et al. (2011). Ptpn11/Shp2 acts as a tumor suppressor in hepatocellular carcinogenesis. Cancer Cell *19*, 629–639.

Beenken, A., and Mohammadi, M. (2009). The FGF family: biology, pathophysiology and therapy. Nat. Rev. Drug Discov. *8*, 235–253.

Buchwald, H., and Gebhard, R.L. (1968). Localization of bile salt absorption in vivo in the rabbit. Ann. Surg. *167*, 191–198.

Chan, R.J., and Feng, G.S. (2007). PTPN11 is the first identified proto-oncogene that encodes a tyrosine phosphatase. Blood *109*, 862–867.

Chiang, J.Y. (2002). Bile acid regulation of gene expression: roles of nuclear hormone receptors. Endocr. Rev. *23*, 443–463.

de Aguiar Vallim, T.Q., Tarling, E.J., and Edwards, P.A. (2013). Pleiotropic roles of bile acids in metabolism. Cell Metab. *17*, 657–669.

Desnoyers, L.R., Pai, R., Ferrando, R.E., Hötzel, K., Le, T., Ross, J., Carano, R., D'Souza, A., Qing, J., Mohtashemi, I., et al. (2008). Targeting FGF19 inhibits tumor growth in colon cancer xenograft and FGF19 transgenic hepatocellular carcinoma models. Oncogene *27*, 85–97.

Fon Tacer, K., Bookout, A.L., Ding, X., Kurosu, H., John, G.B., Wang, L., Goetz, R., Mohammadi, M., Kuro-o, M., Mangelsdorf, D.J., and Kliewer, S.A. (2010). Research resource: Comprehensive expression atlas of the fibroblast growth factor system in adult mouse. Mol. Endocrinol. *24*, 2050–2064.

French, D.M., Lin, B.C., Wang, M., Adams, C., Shek, T., Hötzel, K., Bolon, B., Ferrando, R., Blackmore, C., Schroeder, K., et al. (2012). Targeting FGFR4 inhibits hepatocellular carcinoma in preclinical mouse models. PLoS ONE *7*, e36713.

Georgiev, P., Jochum, W., Heinrich, S., Jang, J.H., Nocito, A., Dahm, F., and Clavien, P.A. (2008). Characterization of time-related changes after experimental bile duct ligation. Br. J. Surg. *95*, 646–656.

Gineste, R., Sirvent, A., Paumelle, R., Helleboid, S., Aquilina, A., Darteil, R., Hum, D.W., Fruchart, J.C., and Staels, B. (2008). Phosphorylation of farnesoid X receptor by protein kinase C promotes its transcriptional activity. Mol. Endocrinol. *22*, 2433–2447.

Haugsten, E.M., Malecki, J., Bjørklund, S.M., Olsnes, S., and Wesche, J. (2008). Ubiquitination of fibroblast growth factor receptor 1 is required for its intracellular sorting but not for its endocytosis. Mol. Biol. Cell *19*, 3390–3403.

Henkel, A.S., Anderson, K.A., Dewey, A.M., Kavesh, M.H., and Green, R.M. (2011). A chronic high-cholesterol diet paradoxically suppresses hepatic CYP7A1 expression in FVB/NJ mice. J. Lipid Res. *52*, 289–298.

Houten, S.M., Watanabe, M., and Auwerx, J. (2006). Endocrine functions of bile acids. EMBO J. *25*, 1419–1425.

Huang, W., Ma, K., Zhang, J., Qatanani, M., Cuvillier, J., Liu, J., Dong, B., Huang, X., and Moore, D.D. (2006). Nuclear receptor-dependent bile acid signaling is required for normal liver regeneration. Science *312*, 233–236.

Inagaki, T., Choi, M., Moschetta, A., Peng, L., Cummins, C.L., McDonald, J.G., Luo, G., Jones, S.A., Goodwin, B., Richardson, J.A., et al. (2005). Fibroblast growth factor 15 functions as an enterohepatic signal to regulate bile acid homeostasis. Cell Metab. *2*, 217–225.

Inoue, Y., Yu, A.M., Yim, S.H., Ma, X., Krausz, K.W., Inoue, J., Xiang, C.C., Brownstein, M.J., Eggertsen, G., Björkhem, I., and Gonzalez, F.J. (2006). Regulation of bile acid biosynthesis by hepatocyte nuclear factor 4alpha. J. Lipid Res. *47*, 215–227.

Jeong, W.I., Jeong, D.H., Do, S.H., Kim, Y.K., Park, H.Y., Kwon, O.D., Kim, T.H., and Jeong, K.S. (2005). Mild hepatic fibrosis in cholesterol and sodium cholate diet-fed rats. J. Vet. Med. Sci. *67*, 235–242.

Kerr, T.A., Saeki, S., Schneider, M., Schaefer, K., Berdy, S., Redder, T., Shan, B., Russell, D.W., and Schwarz, M. (2002). Loss of nuclear receptor SHP impairs but does not eliminate negative feedback regulation of bile acid synthesis. Dev. Cell *2*, 713–720.

Kir, S., Zhang, Y., Gerard, R.D., Kliewer, S.A., and Mangelsdorf, D.J. (2012). Nuclear receptors HNF4α and LRH-1 cooperate in regulating Cyp7a1 in vivo. J. Biol. Chem. *287*, 41334–41341.

Kong, B., Wang, L., Chiang, J.Y., Zhang, Y., Klaassen, C.D., and Guo, G.L. (2012). Mechanism of tissue-specific farnesoid X receptor in suppressing the expression of genes in bile-acid synthesis in mice. Hepatology *56*, 1034–1043.

Li, T., Matozel, M., Boehme, S., Kong, B., Nilsson, L.M., Guo, G., Ellis, E., and Chiang, J.Y. (2011). Overexpression of cholesterol 7α-hydroxylase promotes hepatic bile acid synthesis and secretion and maintains cholesterol homeostasis. Hepatology *53*, 996–1006.

Li, S., Hsu, D.D., Wang, H., and Feng, G.S. (2012a). Dual faces of SH2-containing protein-tyrosine phosphatase Shp2/PTPN11 in tumorigenesis. Fr. Medecine *6*, 275–279.

Li, T., Francl, J.M., Boehme, S., Ochoa, A., Zhang, Y., Klaassen, C.D., Erickson, S.K., and Chiang, J.Y. (2012b). Glucose and insulin induction of bile acid synthesis: mechanisms and implication in diabetes and obesity. J. Biol. Chem. *287*, 1861–1873.

Lu, T.T., Makishima, M., Repa, J.J., Schoonjans, K., Kerr, T.A., Auwerx, J., and Mangelsdorf, D.J. (2000). Molecular basis for feedback regulation of bile acid synthesis by nuclear receptors. Mol. Cell *6*, 507–515.

Lu, Y., Xiong, Y., Huo, Y., Han, J., Yang, X., Zhang, R., Zhu, D.S., Klein-Hessling, S., Li, J., Zhang, X., et al. (2011). Grb-2-associated binder 1 (Gab1) regulates postnatal ischemic and VEGF-induced angiogenesis through the protein kinase A-endothelial NOS pathway. Proc. Natl. Acad. Sci. USA *108*, 2957–2962.

Makishima, M., Okamoto, A.Y., Repa, J.J., Tu, H., Learned, R.M., Luk, A., Hull, M.V., Lustig, K.D., Mangelsdorf, D.J., and Shan, B. (1999). Identification of a nuclear receptor for bile acids. Science *284*, 1362–1365.

Modica, S., Murzilli, S., and Moschetta, A. (2011). Characterizing Bile Acid and Lipid Metabolism in the Liver and Gastrointestinal Tract of Mice. Current Protocols in Mouse Biology *1*, 289–321.

Modica, S., Petruzzelli, M., Bellafante, E., Murzilli, S., Salvatore, L., Celli, N., Di Tullio, G., Palasciano, G., Moustafa, T., Halilbasic, E., et al. (2012). Selective activation of nuclear bile acid receptor FXR in the intestine protects mice against cholestasis. Gastroenterology *142*, 355–365, e1–e4.

Neel, B.G., Gu, H., and Pao, L. (2003). The 'Shp'ing news: SH2 domain-containing tyrosine phosphatases in cell signaling. Trends Biochem. Sci. *28*, 284–293.

Parks, D.J., Blanchard, S.G., Bledsoe, R.K., Chandra, G., Consler, T.G., Kliewer, S.A., Stimmel, J.B., Willson, T.M., Zavacki, A.M., Moore, D.D., and Lehmann, J.M. (1999). Bile acids: natural ligands for an orphan nuclear receptor. Science *284*, 1365–1368.

Potthoff, M.J., Boney-Montoya, J., Choi, M., He, T., Sunny, N.E., Satapati, S., Suino-Powell, K., Xu, H.E., Gerard, R.D., Finck, B.N., et al. (2011). FGF15/19 regulates hepatic glucose metabolism by inhibiting the CREB-PGC-1α pathway. Cell Metab. *13*, 729–738.

Qiao, L., MacLean, P.S., You, H., Schaack, J., and Shao, J. (2006). knocking down liver ccaat/enhancer-binding protein alpha by adenovirus-transduced silent interfering ribonucleic acid improves hepatic gluconeogenesis and lipid homeostasis in db/db mice. Endocrinology *147*, 3060–3069.

Rao, Y.P., Stravitz, R.T., Vlahcevic, Z.R., Gurley, E.C., Sando, J.J., and Hylemon, P.B. (1997). Activation of protein kinase C alpha and delta by bile acids: correlation with bile acid structure and diacylglycerol formation. J. Lipid Res. *38*, 2446–2454.

Rao, A., Haywood, J., Craddock, A.L., Belinsky, M.G., Kruh, G.D., and Dawson, P.A. (2008). The organic solute transporter alpha-beta, Ostalpha-Ostbeta, is essential for intestinal bile acid transport and homeostasis. Proc. Natl. Acad. Sci. USA *105*, 3891–3896.

Russell, D.W. (2003). The enzymes, regulation, and genetics of bile acid synthesis. Annu. Rev. Biochem. *72*, 137–174.

Sayin, S.I., Wahlström, A., Felin, J., Jäntti, S., Marschall, H.U., Bamberg, K., Angelin, B., Hyötyläinen, T., Orešič, M., and Bäckhed, F. (2013). Gut microbiota regulates bile acid metabolism by reducing the levels of tauro-beta-muricholic acid, a naturally occurring FXR antagonist. Cell Metab. *17*, 225–235.

Seok, S., Kanamaluru, D., Xiao, Z., Ryerson, D., Choi, S.E., Suino-Powell, K., Xu, H.E., Veenstra, T.D., and Kemper, J.K. (2013). Bile acid signal-induced phosphorylation of small heterodimer partner by protein kinase Cζ is critical for epigenomic regulation of liver metabolic genes. J. Biol. Chem. *288*, 23252–23263.

Shi, Z.Q., Lu, W., and Feng, G.S. (1998). The Shp-2 tyrosine phosphatase has opposite effects in mediating the activation of extracellular signal-regulated and c-Jun NH2-terminal mitogen-activated protein kinases. J. Biol. Chem. *273*, 4904–4908.

Shi, Z.Q., Yu, D.H., Park, M., Marshall, M., and Feng, G.S. (2000). Molecular mechanism for the Shp-2 tyrosine phosphatase function in promoting growth factor stimulation of Erk activity. Mol. Cell. Biol. *20*, 1526–1536.

Sinal, C.J., Tohkin, M., Miyata, M., Ward, J.M., Lambert, G., and Gonzalez, F.J. (2000). Targeted disruption of the nuclear receptor FXR/BAR impairs bile acid and lipid homeostasis. Cell *102*, 731–744.

Song, K.H., Li, T., Owsley, E., Strom, S., and Chiang, J.Y. (2009). Bile acids activate fibroblast growth factor 19 signaling in human hepatocytes to inhibit cholesterol 7alpha-hydroxylase gene expression. Hepatology *49*, 297–305.

Stroeve, J.H., Brufau, G., Stellaard, F., Gonzalez, F.J., Staels, B., and Kuipers, F. (2010). Intestinal FXR-mediated FGF15 production contributes to diurnal control of hepatic bile acid synthesis in mice. Lab. Invest. *90*, 1457–1467.

Thomas, C., Pellicciari, R., Pruzanski, M., Auwerx, J., and Schoonjans, K. (2008). Targeting bile-acid signalling for metabolic diseases. Nat. Rev. Drug Discov. *7*, 678–693.

Vallim, T.Q.A., and Edwards, P.A. (2009). Bile acids have the gall to function as hormones. Cell Metab. *10*, 162–164.

Vergnes, L., Lee, J.M., Chin, R.G., Auwerx, J., and Reue, K. (2013). Diet1 functions in the FGF15/19 enterohepatic signaling axis to modulate bile acid and lipid levels. Cell Metab. *17*, 916–928.

Wang, L., Han, Y., Kim, C.S., Lee, Y.K., and Moore, D.D. (2003). Resistance of SHP-null mice to bile acid-induced liver damage. J. Biol. Chem. *278*, 44475–44481.

Wang, X., Fu, X., Van Ness, C., Meng, Z., Ma, X., and Huang, W. (2013). Bile Acid Receptors and Liver Cancer. Curr Pathobiol Rep *1*, 29–35.

Yang, F., Huang, X., Yi, T., Yen, Y., Moore, D.D., and Huang, W. (2007). Spontaneous development of liver tumors in the absence of the bile acid receptor farnesoid X receptor. Cancer Res. *67*, 863–867.

Yu, C., Wang, F., Kan, M., Jin, C., Jones, R.B., Weinstein, M., Deng, C.X., and McKeehan, W.L. (2000). Elevated cholesterol metabolism and bile acid synthesis in mice lacking membrane tyrosine kinase receptor FGFR4. J. Biol. Chem. *275*, 15482–15489.

Zhang, Y., Xu, P., Park, K., Choi, Y., Moore, D.D., and Wang, L. (2008). Orphan receptor small heterodimer partner suppresses tumorigenesis by modulating cyclin D1 expression and cellular proliferation. Hepatology *48*, 289–298.

Zhou, W.C., Feng, X.J., Wu, Y.J., Benge, J., Zhang, Z., and Chen, Z.J. (2009). FGF-receptor substrate 2 functions as a molecular sensor integrating external regulatory signals into the FGF pathway. Cell Res. *19*, 1165–1177.

Zhu, H.H., Ji, K., Alderson, N., He, Z., Li, S., Liu, W., Zhang, D.E., Li, L., and Feng, G.S. (2011). Kit-Shp2-Kit signaling acts to maintain a functional hematopoietic stem and progenitor cell pool. Blood *117*, 5350–5361.